Spatially resolved analysis of growth dynamics in pome and drupe fruits of Rosaceae using 3D Gaussian Splatting

Ayame Shimbo[1], Soichiro Nishiyama[1, 2, *], Akane Kusumi[1], Takuya Morimoto[3], Hisayo Yamane[1], Akihiro Itai[3] and Ryutaro Tao[1]

[1] Graduate School of Agriculture, Kyoto University, Sakyo-ku, Kyoto, Kyoto 606-8502, Japan

[2] Research Center for Agricultural Information Technology, National Agriculture and Food Research Organization, Tsukuba, Ibaraki 305-8517, Japan

[3] Graduate School of Life and Environmental Sciences, Kyoto Prefectural University, 74, Kitaina-Yazuma, Seika-town, Soraku-gun, Kyoto 619-0244, Japan

*Corresponding author:

Soichiro Nishiyama (nishiyama.soichiro.8e@kyoto-u.ac.jp)

Abstract

Fruit growth has long been described using single- or double-sigmoid curves; however, these temporal models cannot fully capture the spatial heterogeneity that ultimately shapes a fruit. Here, we present a three-dimensional analysis pipeline that non-destructively tracks spatial fruit growth dynamics from field-collected imaginary. Surface landmarks were drawn, and video recordings were taken throughout development for three pome fruits, apple (*Malus* × *domestica*), Japanese pear (*Pyrus pyrifolia*) and European pear (*Pyrus communis*), and two drupe fruits, peach (*Prunus persica*) and Japanese apricot (*Prunus mume*), to track their motion. Using 3D Gaussian plating, we successfully reconstructed 3D models of the fruits, and the landmark displacement could be measured with high accuracy, with $R^2 \geq 0.98$ when compared to manual recordings. We found a common spatial growth gradient in the longitudinal growth shared in the pomes and drupes of the Rosaceae; proximal (stem-end) regions exhibited more pronounced growth than the distal (stylar) end. An exception was found in European pear (*Pyrus communis*) 'Bartlett,' which showed relatively vigorous growth in the distal region, explaining its distinct shape with expanded distal end. Transverse expansion varied far less than longitudinal expansion, with a possible association with initial fruit morphology. Inter-fruit growth variability peaked in the fastest-growing regions, particularly in the distal area of the European pear, highlighting the link between growth vigor and phenotypic variance. These results provide foundational insights into the developmental dynamics of both pome and drupe fruits of the Rosaceae family, contributing to the optimization of fruit size, shape, and uniformity.

Keywords: Fruit development, fruit shape, non-destructive phenotyping, allometry analysis, growth uniformity

Introduction

Fruit size and shape are key horticultural traits that determine the market value, consumer preference, and post-harvest handling efficiency (Costa et al., 2011; Li et al., 2023). Because agricultural products naturally vary in morphology, products that do not meet the visual standards for these traits are often considered defective (Costa et al., 2011). Therefore, shape uniformity is a critical quality attribute that is ultimately determined by variations in fruit development.

In the Rosaceae family, there are over 100 genera and approximately 3,000 species, including economically important fruits, nuts, ornamental, and timber crops (Shulaev et al., 2008). Rosaceae exhibits diverse fruit types, including drupes, pomes, drupetums, achenes, and achenetums, making it a favored plant family for comparative developmental and evolutionary studies of fruit (Liu et al., 2020). Drupes have fruit flesh derived from the ovary wall and include many agronomically important fruit crops, such as peach (*Prunus persica*), Japanese apricot (*P. mume*), sweet cherry (*P. avium*), and European plum (*P.* x *domestica*). They are also called stone fruits because their endocarp becomes lignified and forms a hard shell that encases one or more seeds. In contrast, pomes, such as apple (*Malus* x *domestica*) and pear (*Pyrus* spp.), have fruit flesh derived primarily from the hypanthium (Pratt, 1988).

Fruit growth is typically modeled as a time-dependent process in one of two major types: a single-sigmoid growth curve, common in pomes (Crane, 1964; Tukey and Young, 1942), and a double-sigmoid growth curve, as observed in drupes (DeJong and Goudriaan, 1989; Nakanishi et al., 1983; Tukey and Young, 1939). The single-sigmoid growth curve is characterized by slow growth at early stages, followed by continuous acceleration during mid-development and gradual deceleration as the fruit reaches maturity. In contrast, the double-sigmoid growth curve is characterized by a lag period

68 after the initial rapid expansion phase, followed by a second growth phase, and a final
69 slowdown as the fruit approaches maturity. In peach, a temporary plateau in fruit growth
70 coincides with endocarp hardening, which is likely caused by the high energy demand
71 required for endocarp lignification (Dardick et al., 2010). Although growth curves can
72 describe the overall growth of an organ well, they are not designed to resolve the localized
73 developmental variations inherent in fruit, which is better characterized through 3D
74 analysis.

75 Recent advancements in spatially resolved analyses of fruit growth have been
76 particularly notable in model plants. For example, a developmental model has been
77 constructed to explain the morphological differences between *Arabidopsis thaliana*
78 (cylindrical fruit) and *Capsella rubella* (heart-shaped fruit) based on analyses of cell
79 growth rates and division orientations (Eldridge et al., 2016). In contrast, such detailed
80 spatial analyses are still limited in fruit trees. This limitation arises due to the large plant
81 size and extended fruit development period of fruit crops, necessitating specialized
82 measurement techniques and introducing variability, while also presenting challenges in
83 applying molecular genetic approaches similar to those conducted in model species.
84 Consequently, a comprehensive understanding of spatial developmental dynamics in fruit
85 trees lags behind that of model plants.

86 Fruit shape and development can be quantified using various image-based
87 methods. For example, the cross-sectional shapes of fruits were objectively and efficiently
88 quantified in different species using predefined descriptors or elliptical Fourier
89 descriptors, which are derived from fruit contours extracted from 2D images (Brewer et
90 al., 2006; Currie et al., 2000; Imai et al., 2024; Wang et al., 2024). However, 2D-based
91 methods often fail to represent the full range of shape features because, in most cases, the
92 2D imaging method acquires shape features that can be seen from only a single

93 perspective of the fruit, which potentially omits biologically important shape features that
94 the original 3D structure possesses. A typical case is the characterization of complex
95 shape development in persimmon (*Diospyros kaki*); complex shape traits such as
96 horizontal and vertical grooves cannot be reliably assessed using 2D methods because of
97 occlusion and covariance with other shape features (Kusumi et al., 2022; Maeda et al.,
98 2018). However, the advent of high-resolution 3D phenotyping pipeline now allows these
99 traits to be captured with precision (Kusumi et al., 2024). Nevertheless, this method still
100 requires imaging in a controlled environment and thus destructive sampling; therefore,
101 continuous, non-destructive 3D measurement of fruit development on the same individual
102 fruit has not been achieved, which ultimately limits the accuracy of spatially resolved
103 growth modeling of the fruit (Kusumi et al., 2025).

104 Recently, several new paradigms have been established for modeling 3D scenes
105 using machine learning approaches. Neural Radiance Fields (NeRF) is a deep learning-
106 based method for reconstructing 3D scenes by modeling a continuous radiance field that
107 maps each 3D point and viewing direction to color and density, enabling the rendering
108 (synthesis) of images from novel viewpoints (Mildenhall et al., 2021). In recent years, a
109 growing number of studies have applied NeRF to fruit tree research, as it enables high-
110 fidelity reconstruction, even under complex lighting conditions and occlusions (Hu et al.,
111 2024; Peng et al., 2025; Wang et al., 2025). In contrast, 3D Gaussian splatting (3DGS) is
112 an explicit, point-based alternative to NeRF (Kerbl et al., 2023). The major difference
113 between NeRF and 3DGS is their representation: NeRF computes the density and color
114 at each point within the scene, whereas 3DGS represents the scene as a collection of
115 spatially distributed Gaussian functions. As a result, 3DGS can construct 3D models more
116 quickly and with a similar or even higher quality than NeRF. Compared to NeRF, the use
117 of 3DGS in plant phenotyping research remains limited but has recently gained attention

(Chen et al., 2025; Shen et al., 2025; Stuart et al., 2025). As both methods can generate high-quality 3D scene models, even from images acquired under outdoor field conditions, they are expected to provide an effective basis for quantitative, full 3D analyses of fruit growth.

In this study, we leveraged machine learning based 3D reconstruction frameworks to continuously and non-destructively track fruit development in the field and to characterize spatial growth heterogeneity in the drupe and pome fruits of Rosaceae. Landmarks were drawn on the fruit surface and their motion on the fruit was recorded on video throughout the growing season. A 3D model of each fruit was then reconstructed, and growth was quantified by tracking the marks over time across different portions of the fruit. Comparable methods have been applied to apple (Skene, 1966), European plum (Khanal et al., 2023) and persimmon (Fujimura, 1935; Kusumi et al., 2025), where they showed vigorous growth in the proximal fruit region. Here, we extended this approach to a broader set of drupes and pomes by incorporating 3D phenotyping. Our approach elucidated the spatial patterns underlying the developmental dynamics shared by drupes and pomes, and provides a fundamental insight and useful pipelines for future research on fruit growth and development.

Materials and methods

Plant materials

This study examined three pome species, apple (‘Fuji’), Japanese pear (*Pyrus pyrifolia* ‘Osa Gold’), and European pear (*Pyrus communis* ‘Bartlett’), planted at the Experimental Farm of Kyoto Prefectural University (Seika, Japan), and two drupe species, Japanese apricot ‘Nankou’ and peach ‘Akatsuki’, planted at the Kyoto Farmstead of the Experimental Farm of Kyoto University (Kyoto, Japan). All were managed according to

143 standard horticultural practices. For apple and pear, fruit thinning was carried out until
144 30–40 days after full bloom (DAFB), leaving one fruit for 4–5 apical buds. In peach,
145 thinning of flower and fruit was carried out accordingly; crop load was limited to 0–1
146 fruit per short fruiting spur and 1–2 fruits per medium- to long-fruiting shoot by the final
147 thinning at 70 DAFB. No crop load control was applied to Japanese apricot.
148
149 **Fruit surface landmarking and field data collection**
150 Landmarks were drawn on the fruit surface using marker ink. The arrangement
151 of the surface landmarking is summarized in Fig 1A. We applied different marking
152 schemes to the pome and drupe. Pome fruits were marked along four stem-stylar lines
153 drawn at 90° intervals. Unlike pome fruits, drupe fruits possess a suture line that
154 introduces additional axis absent in pomes; therefore, they were marked along five stem-
155 stylar lines: two lines on both sides of the suture line, one on the side opposite the suture
156 line, and two between the opposite line and each suture-adjacent line. Three landmarks
157 for pome fruits and four landmarks for drupe fruits were drawn along each line. When the
158 gap between landmarks widened during development, additional landmarks were drawn
159 in between the existing landmarks. In addition, two arbitrarily selected landmarks were
160 drawn in red and manually measured at each observation to verify the measurement
161 accuracy. Fruit growth was recorded once every 1–2 weeks using either an iPhone XR or
162 iPhone 13 (Apple Inc., USA), starting from the stage when the fruit had grown large
163 enough to be marked and continuing until growth ceased. Most of the data collection was
164 conducted during the 2024 growing season. For peach, due to severe fruit drop and
165 insufficient data in 2024, data from both 2024 and 2025 were used for analysis. Each
166 video recording lasted 1–2 min for each fruit, and the fruit was captured from all angles.
167 A ruler was included in each video recording to allow scale calibration. When the tracked

fruit dropped, new fruits were selected and marked following the same procedure.

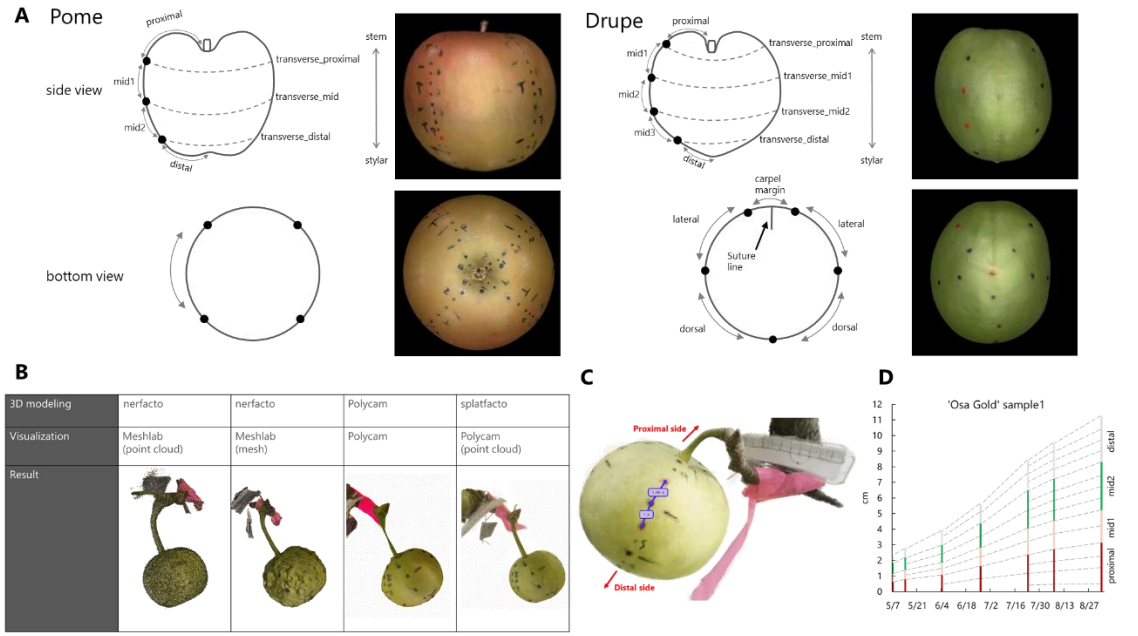

Figure 1. Overview of landmarking methods and 3D modeling for fruit growth analysis. (A) Schematic diagrams of surface landmarking for fruit development analysis. Top: side view, bottom: bottom view. Left: pome, right: drupe. (B) Various combinations of 3D modeling and visualization tools were tested. The best result was obtained using splatfacto from nerfstudio for 3D modeling and Polycam for visualization. (C) Example of distance measurement between surface markers on a fruit using Polycam. After scale calibration with the ruler, the distances between the landmarks were measured. (D) An example of stacked bar graph representing growth in the proximal, mid1, mid2, and distal regions in an 'Osa Gold' fruit.

3D modeling and phenotyping

Each video recording was trimmed to remove unnecessary segments, such as those in which the fruit was absent or swinging owing to wind. Subsequently, image frames were extracted from the video recordings and aligned using either COLMAP

185 v.3.10 (Schönberger and Frahm, 2016) called from Nerfstudio (Tancik et al., 2023;
186 matching method of *vocab_tree* or *exhaustive*) or Metashape v.2.1.3 (Agisoft; default
187 parameters). The alignment software, matching method, and frame extraction interval
188 were optimized for each video recording according to the alignment quality. Subsequently,
189 the 3D model was reconstructed using the Nerfstudio. In Nerfstudio, either the nerfacto
190 pipeline based on NeRF or the splatfacto pipeline based on 3DGS is used. We also tested
191 Polycam application (Polycam Inc., accessed July 12, 2025, https://poly.cam/) for 3D
192 modeling. Meshes generated by nerfacto were visualized using MeshLab 2023.12
193 (Cignoni et al., 2008), whereas splat data generated by splatfacto were visualized using
194 MeshLab or Polycam. Some video recordings were excluded from the analysis because
195 3D reconstruction was not possible, likely because of object motion caused by wind or
196 incomplete view coverage.

197 Scale calibration was performed using the ruler included in the reconstructed 3D
198 models using the scale calibration function of the Polycam. In cases where the ruler was
199 not reconstructed, two red marks whose distances had been measured manually at each
200 recording were used as a reference scale. The distances between the landmarks were then
201 measured using the length measurement function of the Polycam.

202

203 **Data analysis**

204 For longitudinal fruit development analysis, the distances between successive
205 landmarks along a single stem-stylar line that included red marks were measured. The
206 distances within each defined region were then summed to calculate regional length. For
207 pomes, the region from the fruit-pedicel junction to the first landmark was designated as
208 the proximal region, the region between the first and second landmarks as mid1, between
209 the second and third landmarks as mid2, and between the third landmark and the fruit

210 apex as the distal region (Fig 1A). Drupes were partitioned in the same manner, but with
211 one extra landmark, creating an additional mid3 region between mid2 and the distal
212 region (Fig 1A). The regional lengths were then used to calculate the growth rate, which
213 was expressed as a fold-change per week, calculated as

214 $$\text{Fold-change per week} = \left(\frac{L_1}{L_0}\right)^{\frac{7}{\Delta t}},$$

215 where L_0 is the length of the previous observation, L_1 is the length of the current
216 observation, and Δt is the number of days between the two measurements. Measurement
217 dates for sample are listed in Table S1, which also flags missing observations caused by
218 physiological fruit drop or sub-optimal reconstruction quality under certain imaging
219 conditions.

220 For the transverse growth analysis, only the original landmarks (not additional
221 landmarks) were considered. For pomes, three landmarks, (transverse_proximal,
222 transverse_mid, and transverse_distal), were marked on each of the four stem-stylar lines,
223 yielding four measurements per position (Fig 1A); their average was used for further
224 analysis. For drupes, five stem-style lines, for each with four landmarks
225 (transverse_proximal, transverse_mid1, transverse_mid2, and transverse_distal), were
226 grouped into three anatomical portions: carpel margin (along the suture line), lateral, and
227 dorsal (opposite the suture line) sides (see Fig 1A for a diagram). Two values were
228 obtained for each of the lateral and dorsal regions, and their averages were used for the
229 analysis. If a 3D model was incomplete and lacked full 360° coverage, values from the
230 available fruit portion were retained. The fold-change per week was calculated as
231 described for the longitudinal growth analysis.

232 Subsequently, an allometric analysis was conducted to evaluate the relative
233 growth dynamics of each fruit region in relation to total fruit length (Huxley, 1932; Skene,

1966). This analysis was restricted to marked fruits that remained on the tree and were fully imaged throughout the entire growing season. Regional and total lengths were $\log_{10}$-transformed, and for each sample the relationship

$$\log_{10}(\text{regional length}) = a \log_{10}(\text{total length}) + b$$

was fitted by linear regression, where a is the slope, and b is the intercept. This single linear model adequately described the allometric relationship between regional and total fruit lengths in most species; however, the distal region of apple and peach deviated from linearity (see Results). To accommodate this, piecewise linear regression was applied. For each candidate breakpoint c (expressed as $\log_{10}$ total length), the data were split into two subsets at c, and a piecewise linear model was fitted to each segment as:

$$\log_{10}(\text{regional length}) = \begin{cases} a_1 \log_{10}(\text{total length}) + b_1, & if\ \log_{10}(\text{total length}) \leq c \\ a_2 \log_{10}(\text{total length}) + b_2, & if\ \log_{10}(\text{total length}) \geq c \end{cases}$$

The breakpoint c was iteratively shifted across the range of total lengths, and the one yielding the highest mean R^2 across the two segments was selected.

To quantify the inter-fruit variation, each distance value was normalized by setting the landmark distance on the latest common start date to 1. As the measurement dates differed among the samples, the interval between successive observations was uneven. Therefore, spline interpolation was applied to estimate the daily landmark distances. The standard deviation among the fruits over this relative distance was then calculated for each day until the earliest common end date.

Results

Evaluation of in-field 3D fruit measurement methods

The quality of the visualization was evaluated using different combinations of 3D modeling and rendering methods. Among them, the combination of 3D modeling with splatfacto and visualization with Polycam enabled a faster workflow of visually high-quality models (Fig 1B). Using this method, the developmental trajectories of the five fruit species were tracked non-destructively (Supplementary Fig S1). The temporal changes in fruit morphology were successfully captured throughout the developmental timeline. Thereafter, growth in each region was confirmed to be tracked continuously using surface landmarks throughout development in the same sample (Fig 1C and D). Concordance with the manual caliper measurements and with 3DGS-based measurements was high for all species, with coefficients of determination (R^2) ≥ 0.98 (Supplementary Fig S2).

Using this method, the longitudinal growth rates among the five species were compared (Fig 2). In all species, growth was vigorous during the early fruit development stage, followed by a gradual slowdown toward maturity, consistent with typical fruit growth patterns.

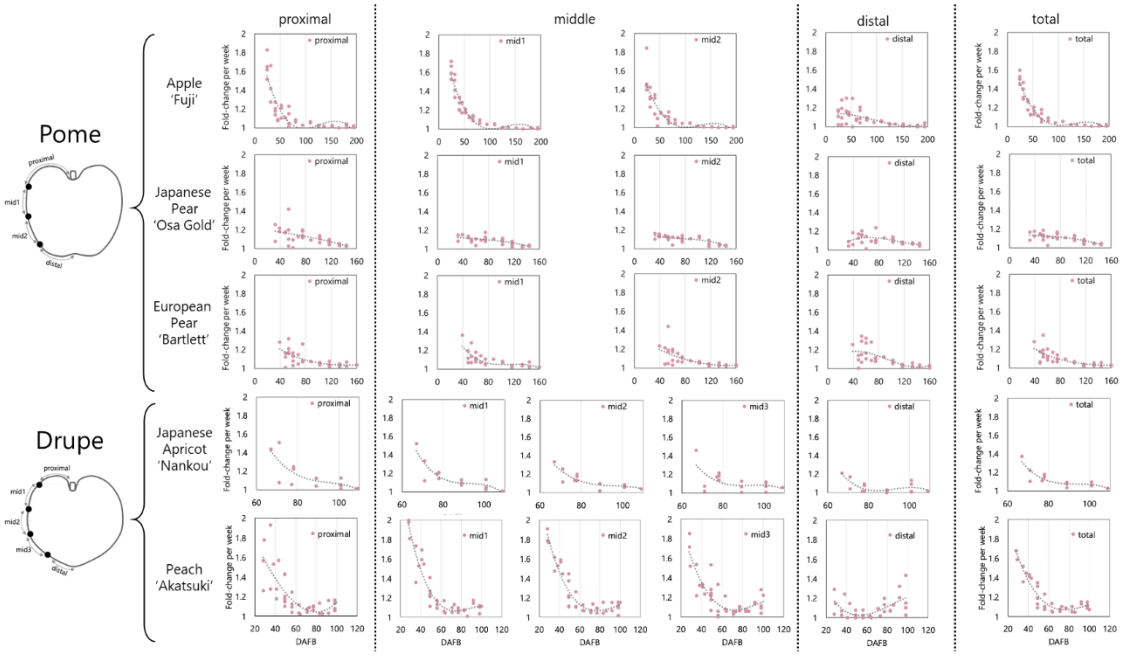

Figure 2. Spatial analysis of longitudinal fruit growth. From left to right: proximal, middle (pome: mid1 and mid2; drupe: mid1, mid2, and mid3), distal, and total (the sum of all regions) values. From top to bottom: Apple 'Fuji', Japanese pear 'Osa Gold', European pear 'Bartlett', Japanese apricot 'Nankou', and Peach 'Akatsuki'.

Comparative analysis of growth rates across fruit regions in pome

In pome fruits, the temporal pattern of longitudinal growth rates was generally similar and declined from the proximal to the distal region, although the pattern and magnitude varied considerably among the species (Fig 2). In apple 'Fuji,' the growth differed markedly between the proximal and distal regions. In particular, growth was more vigorous in the proximal and mid1 regions and slower in the distal region. In Japanese pear 'Osa Gold,' although the growth gradient was relatively smaller, growth in the proximal region was most vigorous, consistent with the pattern observed in apple 'Fuji.' In contrast, in European pear 'Bartlett,' the regional differences in growth were subtle. Compared to apple 'Fuji' and Japanese pear 'Osa Gold,' relatively vigorous growth was observed in the distal region in European pear 'Bartlett,' being consistent with its

enlarged appearance of the distal portion and a larger diameter than that of the proximal region (Supplementary Fig S1).

In contrast to longitudinal growth, spatial variation in transverse growth was relatively modest (Fig 3). In apple 'Fuji,' longitudinal growth in the distal region was clearly less than that in the proximal, mid1, and mid2 regions, whereas transverse growth in the distal region (transverse_distal) was not as limited as in the longitudinal direction and was moderately vigorous. In Japanese pear 'Osa Gold' and European pear 'Bartlett,' the growth patterns among regions were similar between longitudinal and transverse directions; In 'Osa Gold,' transverse growth was most vigorous in the proximal region (transverse_proximal), as also seen in the longitudinal direction. In 'Bartlett,' distal region (transverse_distal) also exhibited vigorous transverse growth.

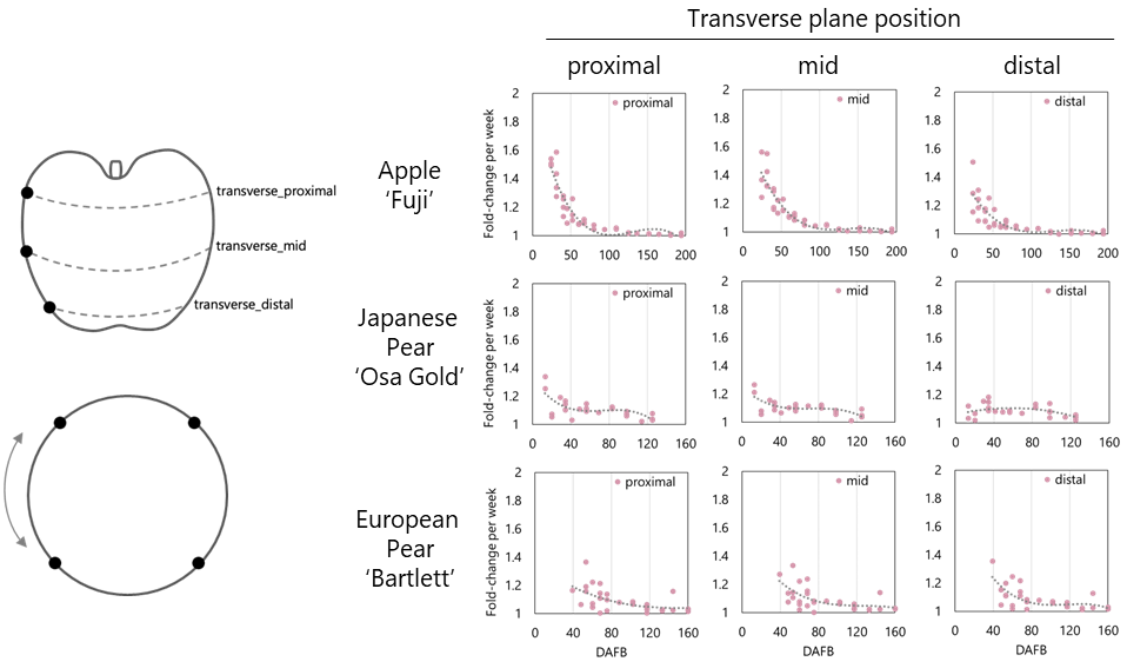

Figure 3. Spatial analysis of transverse growth of pomes. From top to bottom: Apple 'Fuji', Japanese pear 'Osa Gold', and European pear 'Bartlett'. From left to right: transverse_proximal, transverse_mid, and transverse_distal regions.

304 **Comparative analysis of growth rates across fruit regions in drupe**

305 The longitudinal growth patterns were similar between Japanese apricot
306 'Nankou' and peach 'Akatsuki,' in which the proximal region showed more vigorous
307 growth than the distal region (Fig 2). However, the temporal patterns of these two species
308 were different. In Japanese apricot 'Nankou,' growth plateaued during the late stage of
309 fruit development, whereas in peach 'Akatsuki,' growth was stalled at the middle stage
310 but accelerated again at the late stage. Furthermore, in the distal region of peach
311 'Akatsuki,' growth was more vigorous in the late stage than in the early developmental
312 stage.

313 For transverse growth in drupes, spatial analysis was conducted with a focus on
314 the suture line, which serves as a structural axis of growth that was not present in the
315 pomes (Fig 4). The overall growth pattern resembled that observed in the longitudinal
316 direction, with peach 'Akatsuki' exhibiting increased growth during the late
317 developmental stage, whereas Japanese apricot 'Nankou' did not. In 'Nankou,' in contrast
318 to the longitudinal analysis, the distal region (transverse_distal) exhibited transverse
319 growth comparable to other regions. In peach 'Akatsuki,' unlike Japanese apricot
320 'Nankou,' the transverse_distal region showed limited growth compared with the other
321 regions especially during the early developmental stage, consistent with the longitudinal
322 growth trend (Figs 2 and 4). However, during the late developmental stage, recovery of
323 transverse growth was observed particularly in the distal region (transverse_distal). In
324 both species, the regional growth rates along the transverse axis were generally uniform,
325 and no obvious growth variation along the suture line was observed in this study.

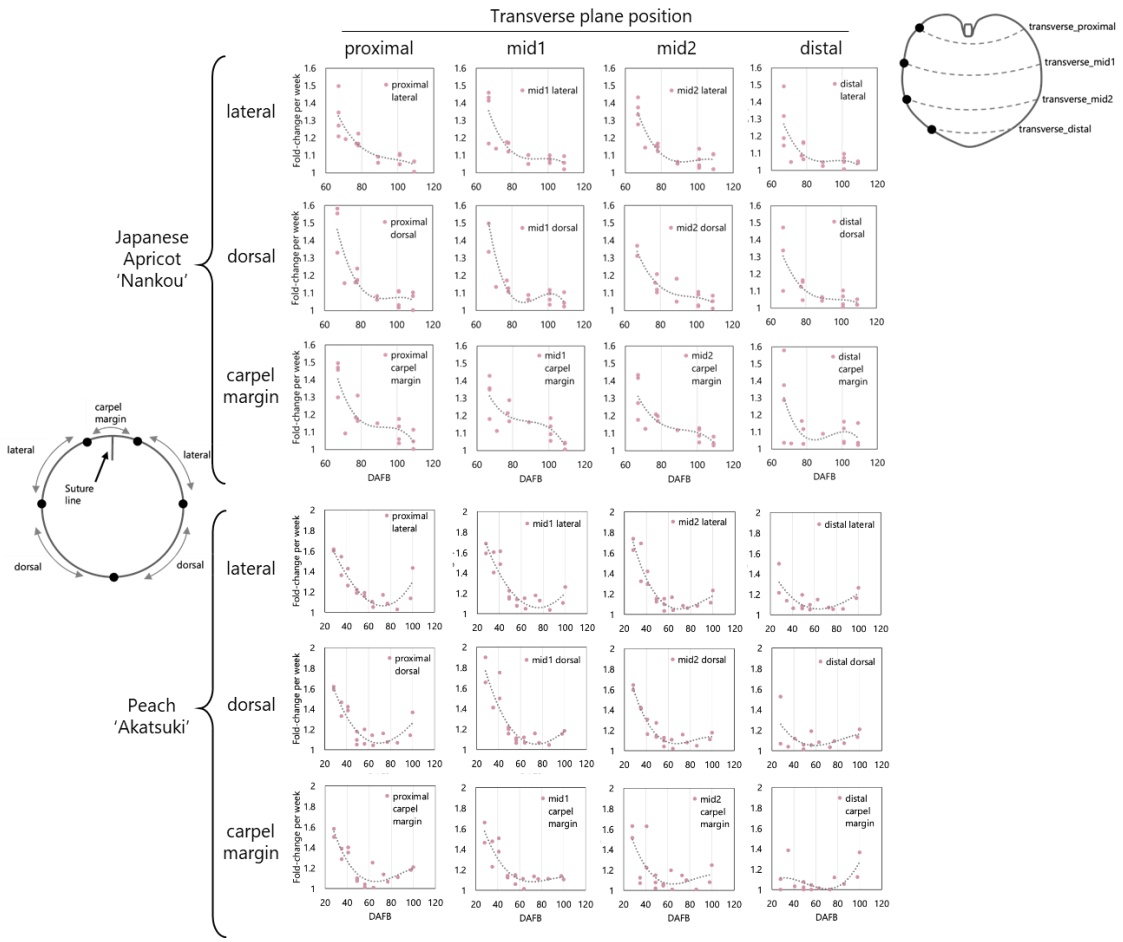

Figure 4. Spatial analysis of transverse growth of drupes. From top to bottom: Japanese apricot 'Nankou', and peach 'Akatsuki', within each species: lateral, dorsal, and carpel margin regions. From left to right: transverse_proximal, transverse_mid1, transverse_mid2, and transverse_distal regions.

Allometric analysis of spatially localized fruit growth

Allometric relationships in regional fruit growth have long been suggested (Barabé and Jean, 1995; Skene, 1966); here we observed allometric relationships between regional growth and total fruit length for each species and region (Supplementary Figs. 3–7). Across species, hyperallometric growth ($a > 1$), in which regional growth was higher relative to the overall fruit, was detected in specific regions (Table 1): proximal

338 and mid1 of apple 'Fuji,' proximal and distal of Japanese pear 'Osa Gold,' distal of
339 European pear 'Bartlett,' proximal-mid2 of Japanese apricot 'Nankou,' and mid1-mid3 of
340 peach 'Akatsuki.' These findings agree with the absolute growth rate analysis (Fig 2),
341 particularly pronounced growth in the distal region of 'Bartlett.'

342 Linear regression fittings were satisfactory for most species and regions, but
343 distal regions of apple 'Fuji' and peach 'Akatsuki' showed poor fits (R^2=0.66 at the
344 lowest; Supplementary Figs 3A and 7A), suggesting a slope shift during development.
345 Piecewise regression (Supplementary Figs 3B and 7B) improved the fitness and revealed
346 a constant trend: an early hypoallometric phase ($a < 1$), in which slower regional growth
347 relative to total fruit length, followed by a late hyperallometric phase ($a > 1$). The
348 breakpoint occurred at the total length of 5-8 cm for 'Fuji' and around 8 cm for 'Akatsuki,'
349 marking a transition in distal growth dynamics. Collectively, these results identify
350 species- (or cultivar-) specific "growth-hotspots" and a critical developmental switch
351 from slower- to faster-than-proportional-expansion in the distal region.

352

353 Table 1. Summary of regional allometry. Regression slopes (a) are shown as mean ± SE
354 (N = 4-5) for each species and region. For the piecewise linear model, slopes are presented
355 separately as pre-breakpoint ($\leq c$) and post-breakpoint ($\geq c$).

	single linear model					piecewise linear model	
	proximal	mid1	mid2	mid3	distal	distal (pre-breakpoint)	distal (post-breakpoint)
Fuji	1.03 ± 0.029	1.11 ± 0.013	0.93 ± 0.029	-	0.77 ± 0.058	0.38 ± 0.088	1.07 ± 0.072
Osa Gold	1.10 ± 0.033	0.89 ± 0.014	0.96 ± 0.018	-	1.05 ± 0.017	-	-
Bartlett	0.97 ± 0.022	0.99 ± 0.022	0.97 ± 0.021	-	1.13 ± 0.070	-	-
Nankou	1.18 ± 0.146	1.15 ± 0.083	1.05 ± 0.048	0.99 ± 0.119	0.58 ± 0.154	-	-
Akatsuki	0.98 ± 0.074	1.13 ± 0.063	1.12 ± 0.045	1.02 ± 0.053	0.53 ± 0.130	0.25 ± 0.043	1.25 ± 0.266

356

357

Spatial analysis of inter-fruit growth variations

Inter-fruit variations in growth trajectories have substantial economic implications, since they influence the fruit uniformity. To quantify these differences at spatial resolution, we applied spline interpolation to estimate daily growth and then normalized each trajectory (see Materials and Methods). The resulting smooth curves enabled day-by-day comparisons of growth among fruits (Supplementary Figs S8-12). The regions showing higher growth variation differed by species (Fig 5). In apple 'Fuji,' Japanese pear 'Osa Gold,' and Japanese apricot 'Nankou,' the variation was greatest in the proximal region. In peach 'Akatsuki,' the variation was greatest in both the proximal and mid1 regions. In contrast, European pear 'Bartlett' showed the greatest variation in the distal region. These regions matched with the regions that exhibited vigorous growth (Fig 2), implying that faster growing regions are intrinsically more prone to inter-fruit variation.

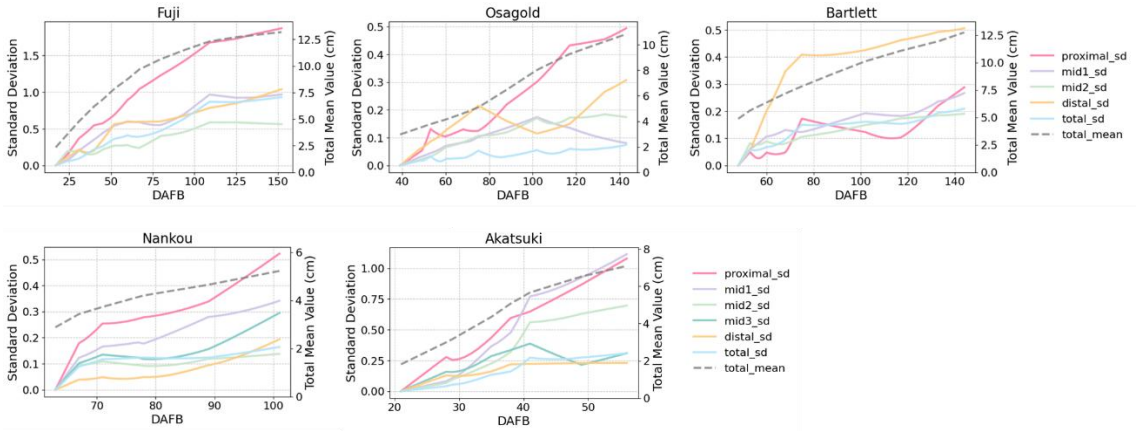

Figure 5. Inter-fruit spatial variation in growth. (A) Pomes (from left to right: apple 'Fuji', Japanese pear 'Osa Gold', and European pear 'Bartlett'). (B) Drupe (left: Japanese apricot 'Nankou'; right: peach 'Akatsuki'). The dashed line indicates the total mean length (cm), and the solid lines indicate the standard deviation for each region.

Discussion

We observed that fruit growth was more vigorous in the proximal region and slower in the distal region in four of the five species (cultivars) examined in this study (Fig 2 and Table 1). This proximal-dominant pattern appeared in both pomes and drupes and aligns with previous reports on the European plum, which also documented enhanced growth near the stem end (Khanal et al., 2023). A classic study in apple showed maximum growth in the middle region and the least growth in the distal region (Skene, 1966), but it divided the fruit surface into six regions, whereas our scheme used four. Despite the difference in regional partitions, the overall conclusions are comparable. A similar gradient has been reported in persimmon, a species phylogenetically distant from Rosaceae (Fujimura, 1935; Kusumi et al., 2025). Future studies applying similar spatial 3D phenotyping apprioach to a wider range of species may help to reveal whether the proximal-dominant growth is conserved across fleshy fruits. In parallel, intraspecific variation in fruit morphology has been well characterized in 2D in various species, including plum (*P. salicina*) (Xia et al., 2023), peach (Guo et al., 2018), apple (Dar et al., 2015) and melon (*Cucumis melo*) (Stepansky et al., 1999); expanding such analyses and resources into the spatial 3D growth are warranted, as it may help reveal the developmental mechanisms driving shape variation.

Among the five species used in this study, European pear 'Bartlett' exhibited a unique growth pattern in which the distal region showed relatively vigorous growth (Fig 2). In addition, the variation in growth was greatest in the distal region, unlike in other species (Fig 5). These growth features may be related to the characteristic fruit shape of 'Bartlett.' Because the fruit shape of 'Bartlett' changes considerably throughout development (Bain, 1961) and tends to lack axial symmetry (Supplementary Fig S1), 2D-based metrics, including second derivative-based quantification of pyriform features

402 (White et al., 2000) and elliptical Fourier descriptors of the fruit section (Wang et al.,
403 2024), provide only a partial description of these morphological changes. Our pipeline
404 complements these approaches by capturing more complex and dynamic morphological
405 characteristics. Given the wide range of shape variations in European pears, including
406 globose, ovate, conical, cylindrical, spindle-shaped, pear-shaped, and inverted heart-
407 shaped forms driven by genotype, nutrition, and environmental influences (Wang et al.,
408 2024; Bayazit et al., 2016), precise and dynamic morphometric methodologies, as
409 exemplified in the present study, may provide valuable insights into the mechanisms
410 underlying shape diversity.

411 Despite the similarity in fruit shapes, apple 'Fuji' and Japanese pear 'Osa Gold'
412 showed different growth patterns especially in the transverse axis (Figs 2 and 3). This
413 difference was likely attributable to variations in fruit morphology during early stages.
414 'Fuji' exhibited an elongated shape at the early developmental stage, which can be
415 subsequently modified by pronounced transverse growth, culminating in a more rounded
416 form (Supplementary Fig S1). In contrast, 'Osa Gold' possessed a naturally rounded
417 morphology from the beginning of development and was considered to exhibit
418 comparatively limited transverse expansion (Supplementary Fig S1). Ultimately, the
419 fruits of both species are likely to have a rounded morphology.

420 In the allometric analysis, we observed growth breakpoints that result in more
421 active growth in the later stage within the distal region of apple 'Fuji' and peach 'Akatsuki'
422 (Table 1). This pattern may suggest that, in the distal part, cell division is not particularly
423 active during the early developmental stages, whereas cell expansion occurs at a similar
424 or even greater level than in other regions during the later stages. One possible
425 explanation is that signals promoting cell division may originate from the proximal (stem-
426 end) side. Although this remains speculative, these findings highlight a potential

developmental mechanism that warrants further experimental validation.

The method developed in this study enabled continuous and non-destructive tracing of fruit growth throughout development and is expected to contribute to elucidating the mechanisms underlying physiological disorders caused by fruit growth gradients, such as cracking and shriveling. For instance, in sweet cherry (*P. avium*), larger fruits tend to crack more easily, and kidney- or heart-shaped varieties with deeper stem cavities retain water longer, thereby increasing the risk of cracking (Simon, 2006). In apple, cultivars exhibiting more vigorous transverse growth during fruit enlargement tend to be more prone to fruit cracking (Yamamoto et al., 1993). In European plum, late-stage rapid growth in the proximal region caused neck shriveling (Khanal et al., 2023). By visualizing spatio-temporal growth, our approach may be applied to dissect such relationships to minimize physiological disorders in the future.

The method developed in this study has three main limitations. First, it could not capture the earliest developmental stages of fruit growth because physical landmarks can only be drawn once the fruit reaches a certain size. Second, although early-stage fruits could still be reconstructed using detectable landmarks (Supplementary Fig S1), the resolution was limited, likely due to the difficulty of reconstructing small objects with 3DGS. Third, in orchard environments, occlusions by branches, leaves, and fruits led to insufficient image data, resulting in difficulties in recovering local details and increased aliasing, as previously noted (Chen et al., 2025). To overcome these limitations, further improvements in the accuracy and robustness of imaging method are required. Moreover, by developing this method into a predictive growth model, it may be possible to visualize spatial variations in growth, without relying on physical landmarks. Such advancements are expected to enable more accurate analyses, even for small fruits.

Conclusion

The 3DGS-based method employed in this study enables the reconstruction of high-quality 3D models of fruit that are both visually realistic and quantitatively accurate, as validated against caliper measurements. This approach allows continuous, nondestructive, region-specific tracking of growth at high precision, including the precise localization of surface features. In Rosaceae, growth is generally more vigorous on the proximal side and slower on the distal side. However, in the European pear, the distal region exhibited relatively vigorous growth, which may have contributed to its unique shape. In addition, the greatest variation in growth among the samples was observed in regions where growth was the most vigorous. These findings may contribute to a better understanding of spatially resolved growth dynamics and morphological diversity of fruit across horticulturally important crops.

Acknowledgment

This research was supported by the Japan Society for the Promotion of Science KAKENHI (grant no. 21KK0269 to SN and no. 24KJ1497 to AK), the JST BOOST Program (grant no. JPMJBY24F7 to SN) and a research grant from the Hirose Foundation to SN.

Competing interests

The authors declare that they have no affiliations with or involvement in any organization or entity with any financial interest in the subject matter or materials discussed in this manuscript.

Author Contributions

SN conceived and designed the study. AS and AK optimized field data collection and collected the data. AS and SN developed the methodology, analyzed the data, and drafted the manuscript. SN, TM, HY, AI and RT prepared plant materials and experimental facilities. All authors read and approved the final version of the manuscript.

References

Bain JM. 1961. Some morphological, anatomical, and physiological changes in the pear fruit (*Pyrus communis* var. Williams Bon Chrétien) during development and following harvest. *Australian Journal of Botany* 9:99–123.

Barabé D, Jean RV. 1995. On the allometric growth of tissues in fruits. *Bulletin of Mathematical Biology* 57: 487–498.

Bayazit S, Caliskan O, Sümbül A. 2016. Morpho-pomological diversity of Turkish pear (*Pyrus communis* L.) accessions in eastern mediterranean region of Turkey. *Acta Scientiarum Polonorum Hortorum Cultus* 15: 157–171.

Brewer MT, Lang L, Fujimura K, Dujmovic N, Gray S, van der Knaap E. 2006. Development of a Controlled Vocabulary and Software Application to Analyze Fruit Shape Variation in Tomato and Other Plant Species. *Plant Physiology* 141: 15–25.

Chen Y, Xiao K, Gao G, Zhang F. 2025. High-fidelity 3D reconstruction of peach orchards using a 3DGS-Ag model. *Computers and Electronics in Agriculture* 234: 110225.

Cignoni, P., M. Callieri, M. Corsini, M. Dellepiane, F. Ganovelli and G. Ranzuglia. MeshLab: an Open-Source Mesh Processing Tool. In: Scarano V, De Chiara R, Erra U, eds. *Proceedings of the Eurographics Italian Chapter Conference*. Geneva,

Switzerland: The Eurographics Association, 129–136.

Costa C, Antonucci F, Pallottino F, Aguzzi J, Sun D-W, Menesatti P. 2011. Shape Analysis of Agricultural Products: A Review of Recent Research Advances and Potential Application to Computer Vision. *Food and Bioprocess Technology* 4: 673–692.

Crane JC. 1964. Growth Substances in Fruit Setting and Development. *Annual Review of Plant Physiology* 15: 303–326.

Currie AJ, Ganeshanandam S, Noiton DA, Garrick D, Shelbourne CJA, Oraguzie N. 2000. Quantitative evaluation of apple (*Malus* × *domestica* Borkh.) fruit shape by principal component analysis of Fourier descriptors. *Euphytica* 111: 221–227.

Dar JA, Wani AA, Dhar MK. 2015. Morphological, biochemical and male-meiotic characterization of apple (*Malus* × *domestica* Borkh.) germplasm of Kashmir Valley. *Chromosome Botany* 10: 39–49.

Dardick CD, Callahan AM, Chiozzotto R, Schaffer RJ, Piagnani MC, Scorza R. 2010. Stone formation in peach fruit exhibits spatial coordination of the lignin and flavonoid pathways and similarity to Arabidopsis dehiscence. *BMC Biology* 8: 13.

DeJong TM, Goudriaan J. 1989. Modeling peach fruit growth and carbohydrate requirements: reevaluation of the double-sigmoid growth pattern. *Journal of the American Society for Horticultural Science* 114: 800–804.

Eldridge T, Łangowski Ł, Stacey N, Jantzen F, Moubayidin L, Sicard A, Southam P, Kennaway R, Lenhard M, Coen ES, et al. 2016. Fruit shape diversity in the Brassicaceae is generated by varying patterns of anisotropy. *Development* 143: 3394–3406.

Fujimura, J. 1935. The research on persimmon fruit development. *Journal of the Japanese Society for Horticultural Science* 6:105–117. (in Japanese)

Guo J, Cao K, Li Y, Yao J-L, Deng C, Wang Q, Zhu G, Fang W, Chen C, Wang X, et al.

2018. Comparative Transcriptome and Microscopy Analyses Provide Insights into Flat Shape Formation in Peach (*Prunus persica*). *Frontiers in Plant Science* 8.

Hu K, Ying W, Pan Y, Kang H, Chen C. 2024. High-fidelity 3D reconstruction of plants using Neural Radiance Fields. *Computers and Electronics in Agriculture* 220: 108848.

Huxley, J. 1932. Problems of relative growth. Cambridge, UK: Cambridge University Press.

Imai A, Nishio S, Takeuchi Y, Terakami S, Takada N. 2024. Image analysis of fruit deformation and its application to breeding in Japanese pear (*Pyrus pyrifolia* (Burm. f.) Nakai). *Tree Genetics & Genomes* 20: 1–7.

Kerbl B, Kopanas G, Leimkuehler T, Drettakis G. 2023. 3D Gaussian Splatting for Real-Time Radiance Field Rendering. *ACM Trans. Graph*. 42: 139:1-139:14.

Khanal BP, Bhattarai A, Aryal D, Knoche M. 2023. Neck shrivel in European plum is caused by cuticular microcracks, resulting from rapid lateral expansion of the neck late in development. *Planta* 258: 1–10.

Kusumi A, Nishiyama S, Tao R. 2024. Three-dimensional fruit growth analysis clarifies developmental mechanisms underlying complex shape diversity in persimmon fruit. *Journal of Experimental Botany* 75: 1919–1933.

Kusumi, A., S. Nishiyama, H. Yamane and R. Tao. 2025. Spatially resolved analysis of longitudinal fruit growth in persimmon (*Diospyros kaki*) via three-dimensional phenotyping. *bioRxiv*. doi: https://doi.org/10.1101/2025.07.17.665444.

Kusumi A, Osako Y, Nakano R, Nishiyama S, Tao R. 2022. Phenotypic evaluation of shape diversity in persimmon fruit using two- and three-dimensional imaging. *Acta Horticulturae* 1338:263–268.

Li Q, Luo S, Zhang L, Feng Q, Song L, Sapkota M, Xuan S, Wang Y, Zhao J, van der

Knaap E, et al. 2023. Molecular and genetic regulations of fleshy fruit shape and lessons from Arabidopsis and rice. *Horticulture Research* 10: uhad108.

Liu Z, Ma H, Jung S, Main D, Guo L. 2020. Developmental Mechanisms of Fleshy Fruit Diversity in Rosaceae. *Annual Review of Plant Biology* 71: 547–573.

Maeda H, Akagi T, Tao R. 2018. Quantitative characterization of fruit shape and its differentiation pattern in diverse persimmon (*Diospyros kaki*) cultivars. *Scientia Horticulturae* 228: 41–48.

Mildenhall B, Srinivasan PP, Tancik M, Barron JT, Ramamoorthi R, Ng R. 2021. NeRF: representing scenes as neural radiance fields for view synthesis. *Commun. ACM* 65: 99–106.

Nakanishi, T., I. Domoto, Y. Sakamura, T. Ichii and M. Sawano. 1983. The Fruit Growth and Seed Gibberellin of Japanese Apricot (*Prunus mume* Sieb. et Zucc.). *The science reports of Faculty of Agriculture, Kobe University* 15:247–253

Peng H, Guo S, Zou X, Wang H, Xiong J, Liang Q. 2025. UAVO-NeRF: 3D reconstruction of orchards and semantic segmentation of fruit trees based on neural radiance field in UAV images. *Computers and Electronics in Agriculture* 237: 110631.

Pratt C. 1988. Apple flower and fruit: morphology and anatomy. In: Janick J, ed. *Horticultural Reviews*, Vol. 10. New York, NY, USA: John Wiley & Sons, 273–308.

Schönberger JL, Frahm J-M. 2016. Structure-from-Motion Revisited. In: 2016 *IEEE Conference on Computer Vision and Pattern Recognition (CVPR)*. 4104–4113.

Shen Y, Zhou H, Yang X, Lu X, Guo Z, Jiang L, He Y, Cen H. 2025. Biomass phenotyping of oilseed rape through UAV multi-view oblique imaging with 3DGS and SAM model. *Computers and Electronics in Agriculture* 235: 110320.

577 Shulaev V, Korban SS, Sosinski B, Abbott AG, Aldwinckle HS, Folta KM, Iezzoni A,
578 Main D, Arús P, Dandekar AM, et al. 2008. Multiple Models for Rosaceae
579 Genomics. *Plant Physiology* 147: 985–1003.
580 Simon, G. 2006. Review on rain induced fruit cracking of sweet cherries (*Prunus avium*
581 L.), its causes and the possibilities of prevention. *International Journal of*
582 *Horticultural Science* 12:27–35.
583 Skene DS. 1966. The Distribution of Growth and Cell Division in the Fruit of Cox's
584 Orange Pippin. *Annals of Botany* 30: 493–512.
585 Stepansky A, Kovalski I, Perl-Treves R. 1999. Intraspecific classification of melons
586 (*Cucumis melo* L.) in view of their phenotypic and molecular variation. *Plant*
587 *Systematics and Evolution* 217: 313–332.
588 Stuart LAG, Wells DM, Atkinson JA, Castle-Green S, Walker J, Pound MP. 2025. High-
589 fidelity wheat plant reconstruction using 3D Gaussian splatting and neural
590 radiance fields. *GigaScience* 14: giaf022.
591 Tancik M, Weber E, Ng E, Li R, Yi B, Kerr J, Wang T, Kristoffersen A, Austin J, Salahi
592 K, Ahuja A, McAllister D, Kanazawa A. 2023. Nerfstudio: a modular framework
593 for neural radiance field development. *arXiv* 2302.04264. doi:
594 https://doi.org/10.48550/arXiv.2302.04264
595 Tukey HB, Young JO. 1939. Histological Study of the Developing Fruit of the Sour
596 Cherry. *Botanical Gazette* 100: 723–749.
597 Tukey HB, Young JO. 1942. Gross Morphology and Histology of Developing Fruit of the
598 Apple. *Botanical Gazette* 104: 3–25.
599 Wang H, Yin H, Li H, Wu G, Guo W, Qi K, Tao S, Zhang S, Ninomiya S, Mu Y. 2024.
600 Quantitative 2D fruit shape analysis of a wide range of pear genetic resources
601 toward shape design breeding. *Scientia Horticulturae* 327: 112826.

Wang J, Wang H, Liu B, Gong J, Zhang Y. 2025. Recognition of Apple Fruit at Maturity Based on Neural Radiance Field and PointNeXt. *Journal of Biosystems Engineering* doi: https://doi.org/10.1007/s42853-025-00265-0.

White AG, Alspach PA, Weskett RH, Brewer LR. 2000. Heritability of fruit shape in pears. *Euphytica* 112: 1–7.

Xia L, Chen L, Chen Y, Huang Z. 2023. Phenotypic Variations in External and Internal Fruit Quality Traits of Different Plum Accessions. *Horticultural Science and Technology* 41: 522–536.

Yamamoto T, Hosoi K, Sasahara I, Satou H. 1993. Cracking Susceptibility and Distribution of Surface Stress of Fruit in Apple Cultivars. *Bulletin of the Yamagata University. Agricultural science* 11: 727–747. (in Japanese)